5

Study of Temperature Dependent Electrical Transport and Low Temperature H_2 Gas Sensors based on ZnO NRs/Si HJ

In this chapter, firstly, temperature dependent electrical transport studies of self-aligned ZnO NR's/Si heterojunction (HJ) and current conduction mechanism at HJ are studied. Barrier height and ideality factor is extracted and their temperature dependent behaviour is revealed using I-V-T characteristics. Furthermore, to understand the nature of HJ and the presence of barrier inhomogeneities at HJ, modified Richardson constant and modified barrier height are also calculated.

In second section, ZnO NR's based sensors are used for low temperature hydrogen sensing. In this process, uniformly distributed well aligned ZnO NRs are deposited on silicon substrate. In addition to this, affirmation of ZnO NR's defect free growth is shown using structural, optical and magnetic characterization. Then hydrogen sensing is performed on ohmic contacted ZnO NRs/Si/ZnO NRs double Schottky junction which shows fast response in sensor and the sensor can work even at low operating temperature for pure hydrogen. The hydrogen sensing mechanism is also proposed at the end of this chapter.

5.1 TEMPERATURE DEPENDENT ELECTRICAL TRANSPORT STUDIES OF SELF-ALIGNED ZnO NRs/Si HETEROJUNCTION (HJ)

In recent years, ZnO NRs and thin film based heterojunction (HJ) were grown upon various substrate such as Si [You *et al.*, 2010; Dhananjay *et al.*, 2007; Dutta and Basak, 2008], Sapphire [Jia *et al.*, 2013] and ITO [Lee *et al.*, 2011]. Best quality Si wafer with large area at low cost have been easily available and superior quality ZnO nanostructure could be possible to deposit on Si substrate. Hence, this incorporation becomes a vital procedure for producing practical applications of ZnO in various electronic and opto-electronic devices [Ye *et al.*, 2006; Zhang *et al.*, 2005; Jeong *et al.*, 2003]. The junction between two materials always plays an important role in semiconductor devices and its performance. Optoelectronic and electronic device's performance have been widely affected by the quality of interface. Normally, temperature dependent current-voltage (*I-V-T*) characteristic is used to explain the conduction mechanism and barrier inhomogeneities at ZnO/Si HJ. One of the important property of semiconductor HJ interface is known as Schottky barrier height (SBH). It calculates mismatch of energy level across the junction interface for majority carrier. Thermionic emission (TE) is always predominating carrier transport mechanism to extract barrier height (ϕ_B) and ideality factor (η) at heterojunction in forward bias current voltage (*I-V*) characteristics. However, experimental temperature dependent *I-V* data for various ZnO based heterostructure shows rectifying behaviour in forward bias [Al-Heniti *et al.*, 2011].

Presence of undesirable nonlinearity in the Richardson plot indicates presence of barrier inhomogeneity at heterojunction. Gaussian distribution of barrier height with thermionic emission theory is one of the effective method to explain temperature dependency of barrier height. The mean barrier height and Richardson constant calculated using Gaussian distribution was found to be close to its theoretical values [Chirakkara and krupanidhi, 2012]. Yilmaz *et al.* in [Yilmaz *et al.*, 2012] analysed ZnO/n-ZnO NR HJ by using standard TE theory with the

assumption of Gaussian distribution of barrier heights. In case of n-ZnO NWs/p-Si HJ diode, higher value of Richardson constant is observed due to presence of barrier inhomogeneity phenomenon [Somvanshi and Jit, 2014].

In this section, effect of temperature on electrical transport behaviour of ZnO NRs/Si HJ has been studied. The experimental results are explained on the basis of the TE model with Gaussian distributions.

5.1.1 Deposition of ZnO NRs and Device Fabrication

ZnO NRs were deposited on 2-inch-Si wafers by RF magnetron sputtering technique as earlier mentioned in chapter 4. Firstly, n-Si (100) substrates (resistivity ~0.01-0.02 ohm-cm) were chemically cleaned followed by dipping in 5% HF to remove the surface oxide. ZnO target with purity of 99.999 % were used as source materials and base pressure of vacuum chamber was maintained up to 1 x 10^{-6} mbar. The deposition was carried out in the presence of pure Ar gas (99.999 %) and chamber pressure was maintained 2 x 10^{-2} mbar during deposition. Substrate temperature, target to substrate distance, RF power and Ar flow rate were kept at 500 ^{o}C, 14 cm, 150 W and 60 sccm, respectively. The duration of NRs deposition was 2 hours. The aluminium (Al) circular contacts of 500 µm diameter were fabricated on ZnO NRs and n-Si by thermal evaporation using a physical mask. Temperature dependent *I-V* characterizations of the device were carried out on probe station with Keithley-2612 system source meter. Table 5.1 shows all deposition parameters used for ZnO NRs/Si HJ fabrication.

Table 5.1: Deposition parameter for ZnO NRs/Si HJ fabrication

Substrate	2 inch n-Si (100)
Sputtering target	ZnO (99.999% purity)
Base pressure	1×10^{-6} mbar
Deposition pressure	2×10^{-2} mbar
Deposition time	2 hour
RF power	150 W
Sputtering gas	Argon (60 sccm)
Substrate temperature	500 °C
Target to substrate distance	14 cm
Metallization technique	Thermal evaporation
Metal contact	Al (500 µm dia)

5.1.2 Structural, Surface Morphology and Optical Characterization of ZnO NRs

Surface morphology of ZnO NRs were studied using FESEM and AFM characterization. Figure 5.1 (a-c) shows typical FE-SEM images in top view, 45^{o} tilted and cross-sectional view of ZnO NRs, respectively. It is clearly seen that the as-grown NRs are vertically aligned and uniformly grown over the entire substrate. The average length, diameter and density of rods are found to be approximately 750 nm, 48 nm and 1.26 x 10^{10} cm^{2}, respectively.

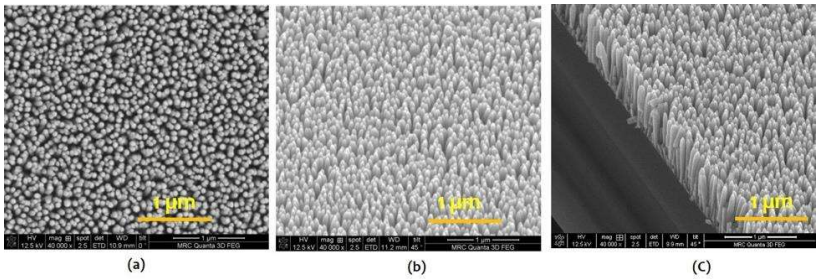

Figure 5.1: FESEM images of ZnO NRs: (a) Top view, (b) 45^{o} Tilted view and (c) Cross-sectional view

AFM characterization also have resemblance with FESEM result of ZnO NRs. Figure 5.2 (a-b) shows 2-D and 3-D view AFM images of the ZnO NRs, which indicates that NRs are uniformly distributed throughout the substrate with average diameter of ~ 48 nm.

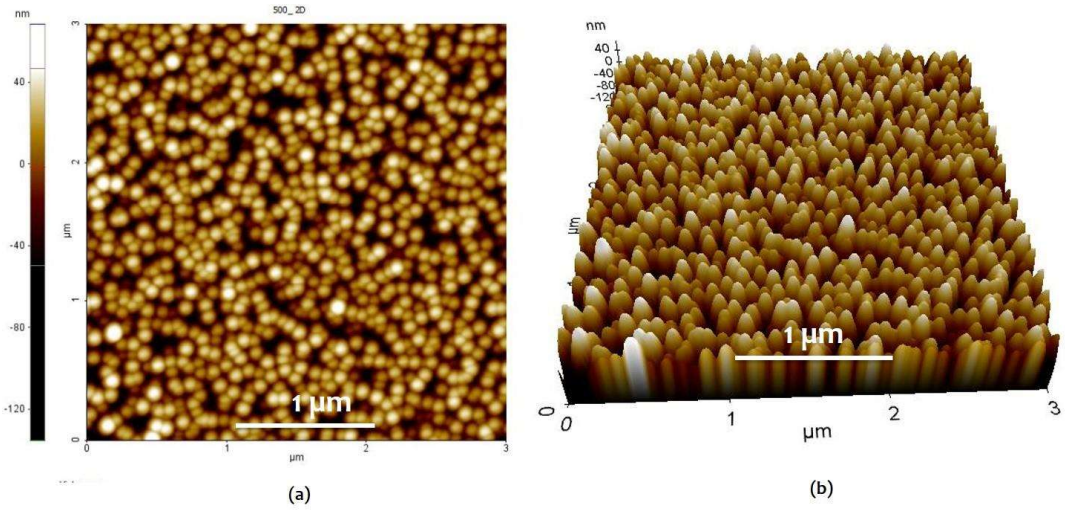

Figure 5.2: (a) 2-D and (b) 3-D View AFM images of the ZnO NRs

The structural characterization of ZnO NRs was evaluated by XRD and are shown in Figure 5.3 (a). As discussed in chapter 4 , the appearance of single peak at 34.64° in the 2θ-ω scan indicates that ZnO NRs are highly c-oriented along [0001] direction of hexagonal wurtzite structure. The full width half maxima (FWHM) of (0002) peak is 12 arcmin, which is consistent with earlier reported value of the ZnO [Singh *et al.*, 2007]. The optical band gap of ZnO NRs were measured by diffused reflectance spectroscopy over UV-Vis spectroscopy and is shown in Figure 5.3 (b). Diffused reflectance spectra was converted into Kubelka-Munk transformed reflectance spectra to calculate band gap of ZnO NRs. The band gap of ZnO NRs was calculated by extrapolating the linear region of $(K*hv)^2$ versus hv graph and was obtained as ~3.24 eV which is close to the literature values [Morales *et al.*, 2007]. The crystalline quality and lattice structures of ZnO NRs were further investigated by micro-Raman spectroscopy which is shown in Figure 5.3 (c). Micro-Raman measurement was analyzed using back scattering geometry from spectra physic with the help of 50 mW argon ion laser corresponding to 514.5 nm phonon excitation. According to Senthil *et al.*, in [Senthil *et al.*, 2009], there are only two Raman active vibration modes namely E_2 (high) and A_1(LO) which are allowed for the c-axis ZnO NWs. From the figure, it can be depicted that except the substrate peaks, a strong peak is appearing at 438 cm^{-1},which attributes to E_2 (high) mode. This indicates that ZnO NRs are crystalline and having hexagonal wurtzite structure. Another weak peak can be seen in the figure appearing at 582 cm^{-1}, which corresponds to E_1(LO) mode. The appearance of this peak confirms the presence of oxygen vacancy and zinc interstitials and such type of the defects are commonly observed in an undoped ZnO [Kung *et al.*, 2012; Umar *et al.*, 2006].

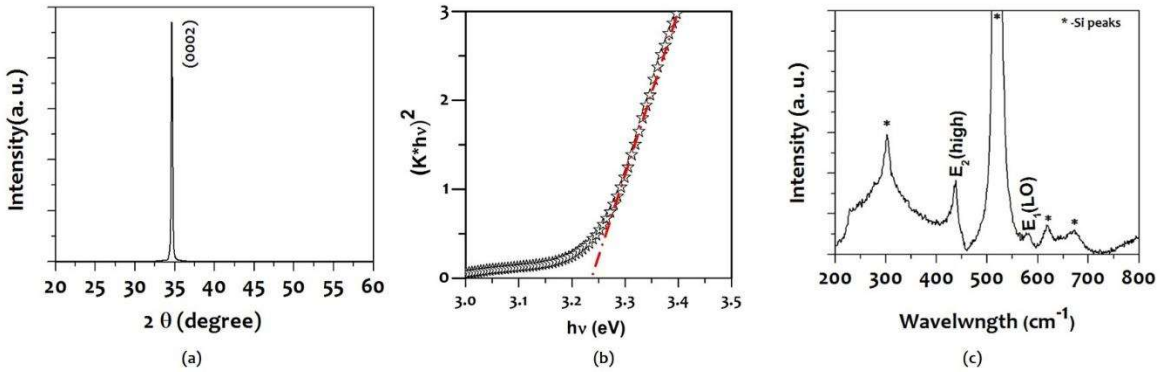

Figure 5.3: (a) XRD 2θ-ω scan, (b) variation of $(K*h\nu)^2$ with photon energy (hν), and (c) Raman spectra of ZnO NRs deposited on n-Si (100) substrate, respectively

5.1.3 Temperature Dependent Current-Voltage (I-V-T) Characteristics

The ZnO NRs/n-Si based heterojunction were obtained by deposited circular ohmic contact of Al on ZnO NRs as well as on Si substrate. The schematic diagram of the device is shown in Figure 5.4 (a). The ohmic nature of Al contacts on Si as well as on ZnO was confirmed by *I-V* measurements and is shown in Figure 5.4 (b). In this I-V characteristics, linear nature of current voltage characteristics on Al/Si/Al and Al/ZnO/Al gives good indication of ohmic contact fabrication on ZnO NRs as well as on Si substrate.

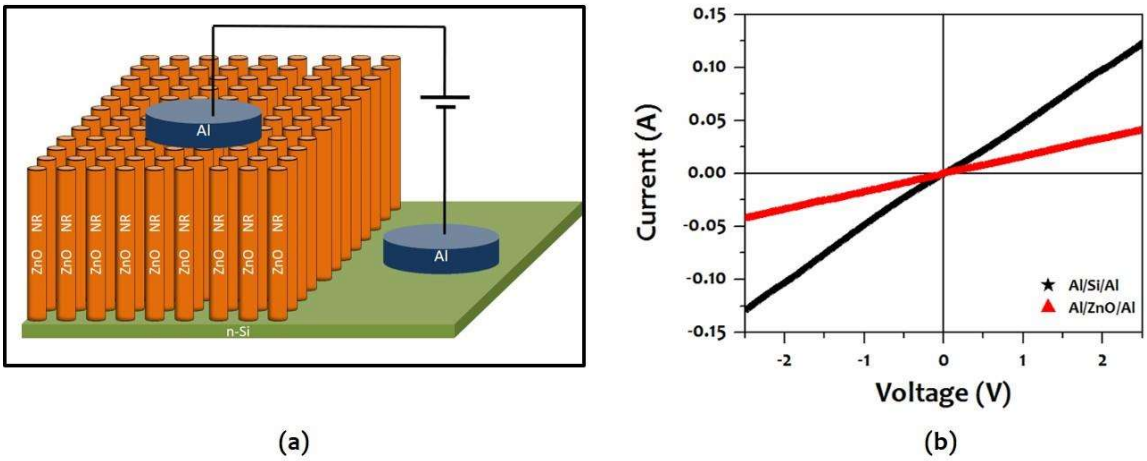

Fig. 5.4: (a) Schematic of the device structure and (b) I-V Characteristics of Al/Si/Al and Al/ZnO/Al contacts

In order to gain innate understanding of ZnO/n-Si heterojunction behaviour, we have studied ideal schematic diagram of the heterojunction, which can be explained by Electron Affinity Model (EAM) [Tansley and Owen, 1098; Dutta and Basak, 2008; Aksoy and Caglar, 2012]. Figure 5.5 shows energy band diagram of ZnO/n-Si HJ (a) before and (b) after thermal equilibrium. When these two semiconductors formed a HJ due to alignment of fermi energy levels, band bending takes place.

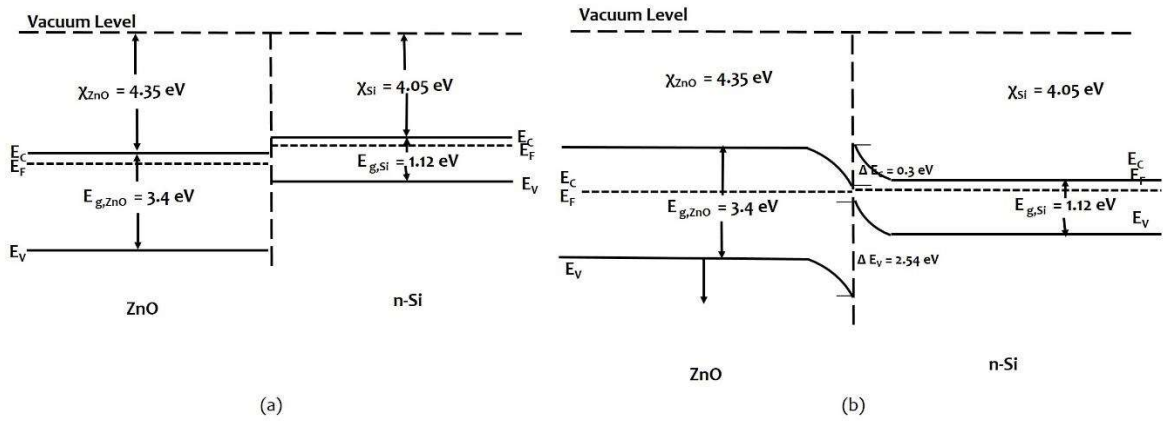

Figure 5.5: Energy band diagram of ZnO/n-Si heterojunction (HJ) (a) Before and (b) After thermal equilibrium

It is clearly seen that both semiconductors have unequal band gap and electron affinities which leads to the formation of band discontinuities or band offset at heterojunction. The current transport properties at heterojunctions are highly influenced by these band offsets. By keeping constant fermi level, we extract difference in energy band gap ΔE_g which is basically sum of valance band offset ΔE_V and conduction band offset ΔE_C. Due to smaller value of conduction band offset as compared with valance band offset value, electrons flow as majority carrier from Si to ZnO at HJ. Conduction band and valance band offsets are calculated by using EAM model:

$$\Delta E_C = \chi_{ZnO} - \chi_{Si} \tag{5.1}$$

$$\Delta E_V = E_{g,ZnO} - E_{g,Si} + \Delta E_C \tag{5.2}$$

where χ_{ZnO}=4.35, χ_{Si}=4.05, $E_{g,ZnO}$=3.24 eV , $E_{g,Si}$=1.12 eV. The value of conduction and valence band offsets are found to be ~0.3 eV and ~2.42 eV, respectively.

Electrical properties of ZnO/Si heterojunction were also analysed using temperature dependent I-V characteristics which gives complete information about junction barrier and current conduction mechanism. Figure 5.6 (a) shows room temperature I-V characterization of n-ZnO NRs/n-Si heterostructure on logarithmic scale and its I-V shows rectifying behaviour which reveals formation of Schottky barrier at ZnO NRs/n-Si HJ. The current rectification ratio is calculated to be 3.6 at 2.5 volt and leakage current to be 3.5 mA. As temperature increases, forward bias current increases with decrease in turn on voltage.

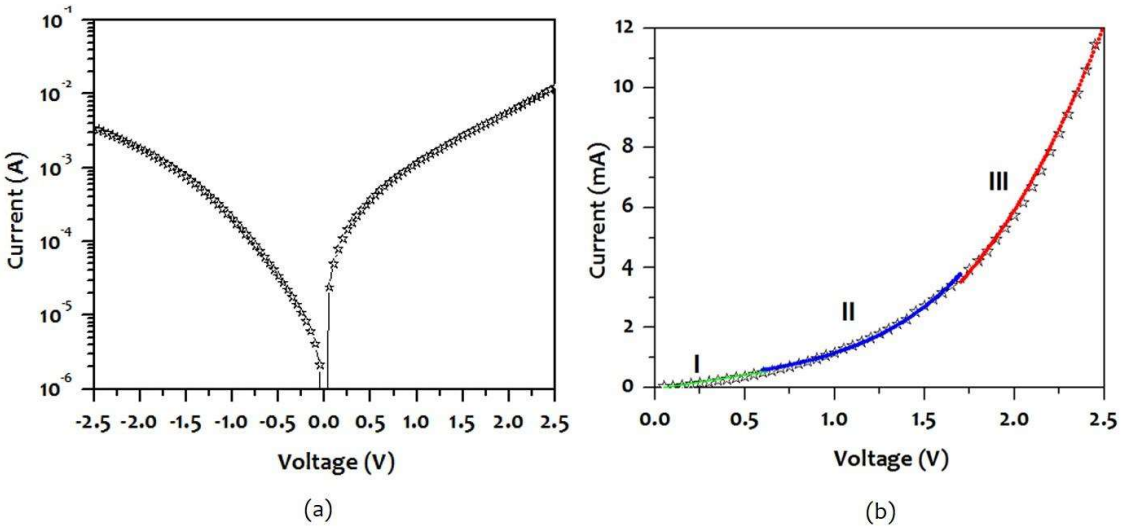

Figure 5.6: (a) Room temperature I-V characteristics of ZnO NRs/Si HJ and (b) Current conduction mechanism in forward bias I-V plot of ZnO NRs/Si HJ

The current conduction mechanism of ZnO NRs/n-Si HJ in forward bias condition at room temperature is shown in Figure 5.6 (b). From the figure, three distinct regions (I, II and III) can be seen, where current strongly depends on the applied voltage. For region I (V ≤ 0.6 V), current obeys Ohmic law in which current increases linearly with voltage ($I \sim V$) due to thermally generated carrier tunnelling where density of injected carrier has been very small in comparison to thermally generated free carrier [Chen *et al.*, 2006]. For region II (0.6 < V ≤ 1.65 V), current exponentially increases with voltage which shows relation as $I \propto \exp(\alpha V)$. This mechanism is usually observed in wide band-gap semiconductor heterojunction diode due to recombination tunnelling mechanism [Ghosh and Basak, 2007]. The α =1.69 V^{-1} was calculated by using exponential fitting in this region. Due to the presence of lattice defects and band discontinuities at HJ, these interface states act as recombination centre for charge carrier. These recombination charge centres provide tunnelling recombination path which then results as band tunnelling. For region III (1.65 < V ≤ 2.5 V), current increases with voltage and satisfies power law ($I \propto V^n$) where n=3.3. In this region, current follows space charge limited conduction mechanism in which current conduction through heterojunction is due to single charge carriers (electrons) [Xiao-Yun *et al.*, 2012]. Higher value of power coefficient (n=3.3) gives indication about trap limited space charge limited conduction (SCLC) mechanism where distribution of traps at HJ is exponential and density of injected electrons is higher than thermally generated free electron carries [Shi *et al.*, 2016].

For detailed investigation of electrical transport through ZnO/n-Si heterojunction, temperature dependent current voltage characterization have been carried out with varying temperature range from 120-300 K by steps of 30K. Forward bias *I-V* characteristics of ZnO NRs/n-Si heterostructure were measured at different temperatures in the temperature range of 120-300 K and is shown in Figure 5.7. This forward bias I-V characteristics shows temperature dependent current conduction behaviour. It is also observed that for a fixed applied voltage bias, forward bias current increases as temperature increases. In heterojunction devices, at Schottky junction, various carrier transport mechanisms are present such as thermionic emission (TE), Trap field emission (TFE), carrier recombination / generation in depletion region, minority carrier injections and carrier tunnelling [Sze and Ng, 2007]. Usually, in certain temperature and voltage regions, one of the above mentioned mechanism dominates. As discussed earlier, forward bias

current increases as operating temperature increases from 120K to 300K at constant applied voltage and gives indication of presence of thermionic emission conduction mechanism at HJ.

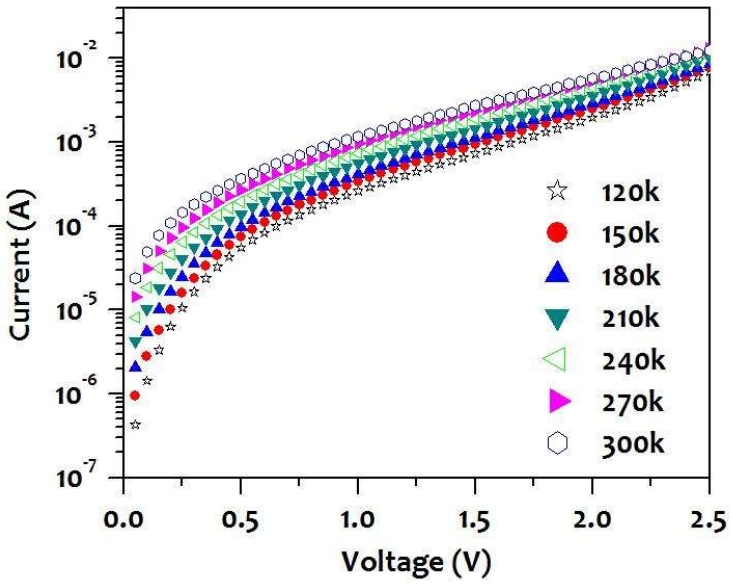

Figure 5.7: Forward bias temperature dependent I-V characteristics in temperature range varying from 120-300 K with incremental steps of 30K

Using thermionic emission model, Schottky barrier height (ϕ_B) and ideality factor (η) for the ZnO NRs/Si HJ are calculated by fitting linear region of forward bias *I-V* characteristics. The *I-V* characteristics of n-ZnO NRs/n-Si HJ is given by [Quemener *et al.*, 2012; Somvanshi and Jit, 2013]:

$$I = I_O \left\{ \exp\left(\frac{qV}{\eta kT} \right) - 1 \right\} \tag{5.3}$$

where η is the ideality factor and I_o is reverse saturation current given by following relation:

$$I_o = AA^* T^2 \exp\left(\frac{-q\phi_B}{kT} \right) \tag{5.4}$$

Here, A^* is Richardson's constant (~ 112 $Acm^{-2}K^{-2}$ for Si), *A* is contact area, *q* is electron charge, T is measurement temperature in Kelvin, k is Boltzmann constant and ϕ_B is effective Schottky barrier height. The ideality factor (η) and effective barrier height (ϕ_B) of Schottky barrier are calculated by fitting linear region of the forward bias using equation 5.3 and observed temperature dependent nature of barrier height as well as ideality factor. Figure 5.8 depicts that barrier height and ideality factor varies with change in temperature. It can be seen from figure that barrier height increases and ideality factor decreases with temperature ranging between 120-300K. The barrier height and ideality factor varies from 0.24 eV to 0.54 eV and 5.5 to 3.5, respectively for change in temperature from 120 to 300 K.

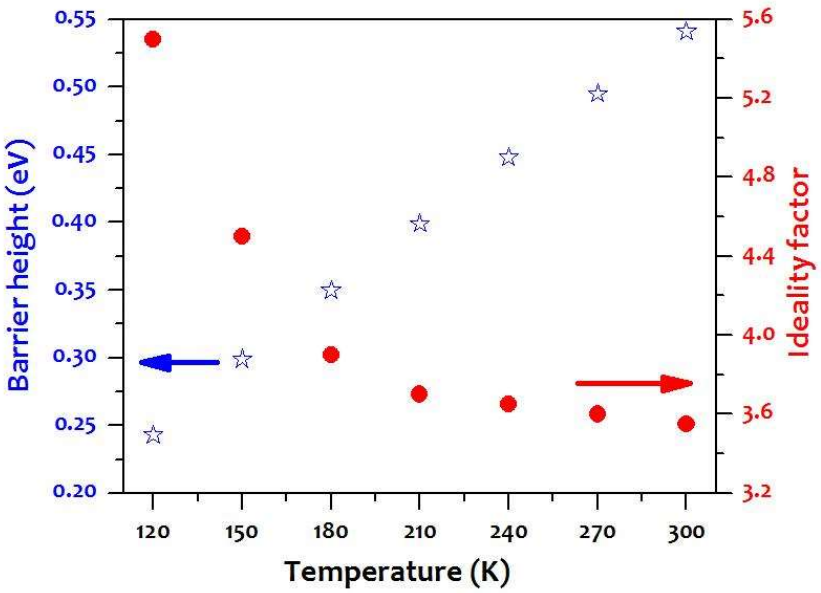

Figure 5.8: Schottky barrier height and ideality factor varying with operating temperature

Because of inhomogeneities and presence of defects at heterojunction, barrier height shows temperature dependent behaviour [Yilmaz *et al.*, 2012; Somvanashi and Jit, 2014; Werner and Cuttler, 1991]. Chirakkara and Krupanidhi in [Chirakkara and Krupanidhi, 2012] described that the barrier height for n-ZnO/p-Si HJ varies from 0.60 eV to 0 .76 eV as temperature is increased from 300K to 390K. At low temperature, electrons are able to surmount the lower barriers and current transport is dominated by current flowing through the defects or intermediate states at ZnO NRs/Si interface due to which, lower Schottky barrier height is obtained at low temperature for majority carrier. As the temperature increases, more electrons gain sufficient energy to surmount the higher barrier and as a result, dominant barrier height increases with temperature [Karatas *et al.*, 2003]. Table 5.2 gives the value of barrier height and ideality factor of ZnO/n-Si Schottky heterojunction obtained by thermionic emission (TE) model. Larger value of ideality factor than its ideal value (η=1) indicates recombination of electron and holes in depletion region. This non ideal behaviour of Schottky junction indicates the presence of barrier inhomogeneities at HJ.

Table 5.2: The value of barrier height and ideality factor of ZnO/n-Si HJ using TE model

Temperature (K)	φ_B(eV)	η
120	0.24	5.5
150	0.30	4.50
180	0.35	3.90
210	0.40	3.70
240	0.45	3.65
270	0.50	3.60
300	0.54	3.55

5.1.4 Effect of Barrier Inhomogeneities (BH) on Effective Barrier Height, Ideality Factor and Richardson Constant

Initially, we determined Schottky barrier height at semiconductor-semiconductor heterojunction assuming that the existing pure thermionic emission conduction mechanism has

no series resistance. Thus, calculated barrier height strongly depends on reverse saturation current I_o and the Richardson constant (A^*) for given operating temperature as mentioned in Equation 5.4. Calculated barrier height may give ambiguity in results due to its dependency on Richardson constant. The Richardson constant strongly depends on operating temperature [Semple *et al.*, 2016]. Hence, for calculating precise value of Schottky barrier height, firstly, we had to calculate actual value of Richardson constant in operating temperature range. Non-ideal behaviour of n-ZnO NRs/n-Si HJ diode can be explained by Richardson plot ($\ln(I_o/T^2)$ versus q/kT) using rearrangement of reverse saturation current equation

$$\ln\left(\frac{Io}{T^2}\right) = \ln\left(AA^*\right) - \frac{q\phi_B}{kT} \tag{5.5}$$

By linear fitting of Richardson plot for different temperature range, we get Richardson constant and barrier height. Figure 5.9 shows temperature dependent Richardson plot [$\ln(I_o/T^2)$ versus q/kT] for 120-300K temperature region. Richardson plot gives two linear regions for two different temperature ranges of 120-180K and 210-300K. The calculated values of Richardson constant (A^*) and barrier height (ϕ_B) for first region (120-180K) are 1.02 x10^{-7} Acm^{-2}K^{-2} and 0.028 eV, respectively. Whereas, corresponding value for the second region (210-300K) are 1.20 x 10^{-6} Acm^{-2}K^{-2} and 0.067 eV, respectively. Major changes in the Richardson constants indicates the presence of barrier inhomogeneities at HJ, which results in large deviation in barrier height for both temperature ranges.

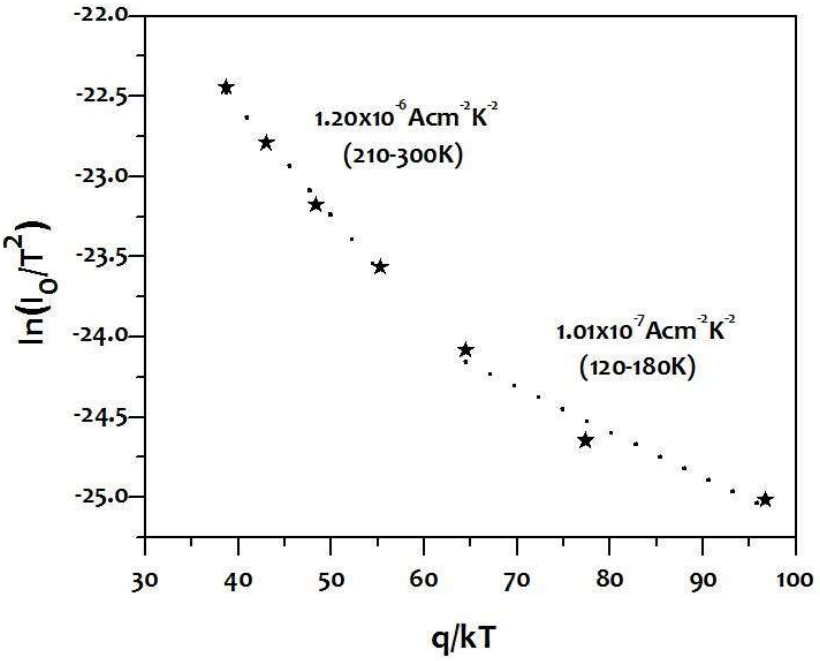

Figure 5.9: Temperature dependent Richardson plot of $\ln(I_o/T^2)$ versus q/kT for 120-300K operating temperature range

Therefore, due to presence of dangling bands and defects at interface, these barrier inhomogeneities leads towards larger deviation in Richardson constant value for different operating temperature ranges. These barrier inhomogeneities creates lower barrier height and higher barrier height areas across the interface. When current flows across the junction, it

preferably passes through lower barrier height region in spite of its actual barrier height area. To obtain correct value of Richardson constant and effective barrier height at HJ, barrier height inhomogeneities correction is required. Thug in [Tung, 1992] described Gaussian distribution of barrier height using thermionic equation with mean barrier height ($\overline{\phi_B}$) and standard deviation (σ) of barrier height. Small value of standard deviation is observed for less barrier inhomogeneities at junction. Gaussian distribution of barrier height can be given as [Asil *et al.*, 2009]

$$P\left(\phi_B\right) = \frac{1}{\sigma\sqrt{2\pi}} \exp\left[-\frac{\left(\phi_B - \overline{\phi_B}\right)^2}{2\sigma^2} \right] \tag{5.6}$$

where the effective barrier height can be represented as a function of q/2kT, given as

$$\phi_B = \overline{\phi_B} - \frac{q\sigma^2}{2kT} \tag{5.7}$$

Figure 5.10 shows effective barrier height versus q/2kT plot as function of temperature. By using linear fitting, intercept point of straight line at zero gives mean barrier height ($\overline{\phi_B}$) and slope of line gives standard deviation (σ^2). Observation of two different linear region having temperature range of 120-180 K and 210-300 K indicates double Gaussian distribution of barrier height at n-ZnO NRs/n-Si HJ [Arslan *et al.*, 2009]. For these two Gaussian regions, calculated value of mean barrier height and standard deviation (σ^2) are 0.55 ± 0.01 eV and 0.0065 (120-180K for region I) and 0.86 ± 0.02 eV and 0.017 (210-300K for region II), respectively. At low temperatures, electron does not have enough energy to surmount the barrier and it will tunnel through the defects at the interface. Hence, at low temperature of 120–180K, the current is dominated by field effect (FE) mechanism due to tunnelling-dominated carrier transports. At higher temperature (210-300 K), the carriers have enough energy to surmount the barrier and current transport is dominated by TE mechanism.

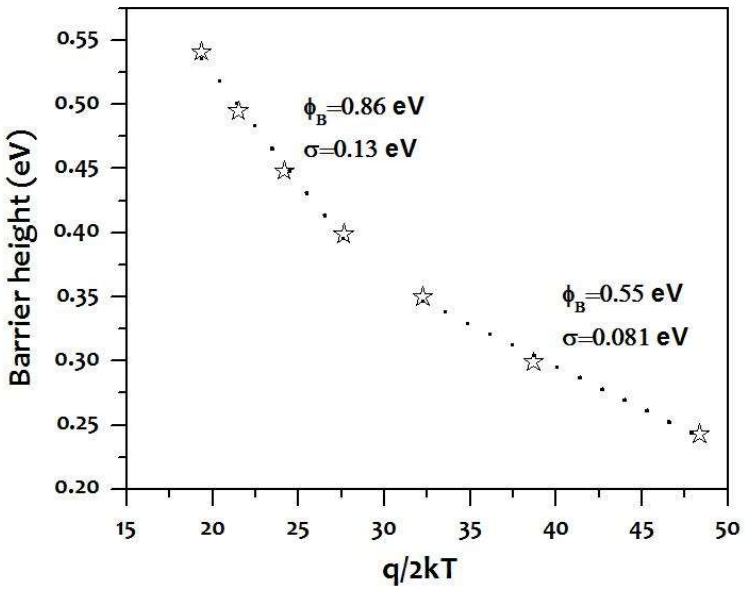

Figure 5.10: Plot of effective barrier height versus q/kT

For the calculation of Richardson constant, Gaussian distribution is applied to the Richardson constant equation that gives modified Richardson constant equation as stated below:

$$\ln\left(\frac{Io}{T^2}\right)-\left(\frac{q^2\sigma^2}{2k^2T^2}\right)=\ln\left(AA^*\right)-\frac{q\overline{\phi_B}}{kT} \tag{5.9}$$

Modified Richardson plot of $\ln\left(\frac{Io}{T^2}\right)-\left(\frac{q^2\sigma^2}{2k^2T^2}\right)$ versus q/2kT is shown in Figure 5.11.

Mean barrier height and Richardson constant were calculated from the slope and intercept of the linear fitted curve. Richardson constants and mean barrier heights are 136.3 $Acm^{-2}K^{-2}$ and 0.55 eV for region I (120-180K) and 123.4 $Acm^{-2}K^{-2}$ and 0.86 eV for region II (210-300K), respectively. Mean barrier height value has resemblance to mean barrier height obtained from Gaussian distribution of barrier height plot. At higher temperature range (210-300 K), Richardson constant value is more accurate to the theoretical value of Richardson constant of n-Si (112 $Acm^{-2}K^{-2}$) than lower temperature region (120-180K). Somvanshi and Jit [Somvanshi and Jit, 2014] also described the deviated of Richardson constant from 32 $Acm^{-2}K^{-2}$ to 49 $Acm^{-2}K^{-2}$ for n-ZnO. Consideration of barrier inhomogeneities distribution at junction gives more appropriate value of Richardson constant. Quemener *et al.* [Quemener *et al.*, 2012] fabricated HJ by atomic layer deposition and the barrier heights obtained were 0.61eV and 0.52 eV for n-ZnO/n-Si HJ and n-ZnO /p-Si HJ, respectively for temperature range 180-280K.

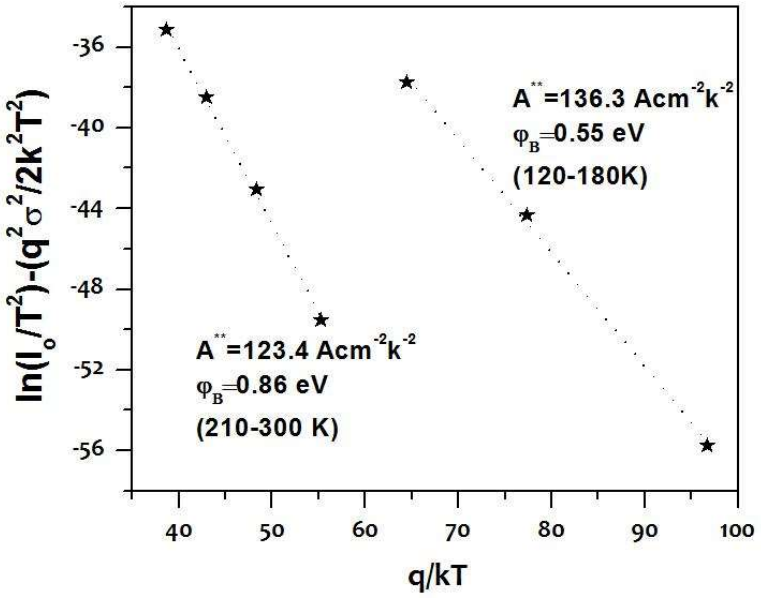

Figure 5.11 : Modified Richardson plot of $\ln\left(\frac{Io}{T^2}\right)-\left(\frac{q^2\sigma^2}{2k^2T^2}\right)$ versus q/2k

In the present study, the barrier height extracted using Gaussian distribution and modified Richardson plot for higher temperature range (210-300K) gives mean barrier height 0.86 eV which is slightly higher than earlier reported value (p1,29). The higher barrier height value

could be due to the presence of a thin oxide layer (<3 nm) between ZnO and Si, which is commonly found in RF sputtered HJs.

5.2 ZnO NANORODS FOR LOW TEMPERATURE HYDROGEN SENSOR APPLICATIONS

Till today, majority H_2 sensors are operating at higher temperature that is above 150 °C due to enhanced chemisorbed reactions that gives enhanced sensitivity and fast response/ recovery time. Sensors with high operating temperature also boosts molecular desorption reactions which removes all byproduct from gas sensing layer and enhances sensor's repetitive capabilities. Due to highly explosive nature of H_2 at high temperature, low ignition energy and its non-adorable nature demands to develop H_2 sensors with low operating temperature. In hydrogen sensor, Schottky barrier height at heterojunction is highly influenced by adsorption/desorption of gases, which enhance the sensitivity of the device [Jia *et al.*, 2016; Ju *et al.*, 2015; Shafiei *et al.*, 2010]. In various gas sensors with intrinsic defects (oxygen vacancies) may enhance sensing response by using these vacancies as gas adsorptions sites at elevated sensor temperature (>150 °C) [Zhang *et al.*, 2012; Wildfire *et al.*, 2014].

In the present work, the hydrogen sensing characteristic of the ZnO NRs/Si/ZnO NRs double Schottky junctions is explained. Electrical characterization is performed at room temperature using I-V characterization and barrier height of ZnO NRs/ Si/ ZnO NRs double schottky junction as well as on ZnO NRs/ Si schottky junction in forward bias is calculated. Then hydrogen gas sensor's response and response/recovery time is also studied at low operating temperature. Further more gas sensing mechanism is also proposed.

5.2.1 ZnO NRs based Hydrogen Sensor Fabrication

Vertically aligned, uniformly distributed ZnO nanorods (NRs) were deposited on n-Si (100) wafer using RF-sputtering technique. ZnO target (99.999% purity) was used for NRs deposition in presence of pure argon (99.999% purity). During deposition, chamber pressure and substrate temperature were maintained at 2×10^{-2} mbar and 500 ^{o}C, respectively, with a constant Ar gas flow of 60 sccm. RF power was maintained at 150W and target to substrate distance around ~14 cm. Deposition time was kept 2 hours. Furthermore, for confirmation of defect free nature of ZnO NRs and structural characterizations were carried out using XRD and TEM. Surface morphologies and optical characterizations were studied using FESEM and photoluminescence (PL) spectra. Magnetic properties were studied at room temperature using Vibrating Sample Magnetometer (VSM).

Ohmic contact of Au(200nm)/Ti(20nm) metal contact on ZnO NRs and Al(200nm) on Si substrate of 500 nm diameters were deposited by thermal evaporation using physical mask. ZnO NRs/n-Si /ZnO NRs devices were fabricated by selective wet chemical etching. For H_2, gas sensing measurements were performed in vacuum chamber with 2×10^{-3} mbar chamber pressure. ZnO nanorods/n-Si /ZnO NRs device was heated up at a constant temperature of 70°C and gas flow was controlled using mass flow controller. Pure hydrogen was used for hydrogen sensing. Resistive response curve with respect to time was measured. Table 5.3 shows deposition parameter of ohmic contacted ZnO NRs based hydrogen sensor.

Table 5.3: Deposition parameter for ohmic contacted ZnO NRs/Si /ZnO NRs DHJ based hydrogen sensor

Substrate	2 inch n-Si (100)
Sputtering target	ZnO (99.999% purity)
Base pressure	1×10^{-6} mbar
Deposition pressure	2×10^{-2} mbar
Deposition time	2 hour
RF power	150 W
Sputtering gas	Argon (60 sccm)

Substrate temperature	500 °C
Target to substrate distance	14 cm
Metallization technique	Thermal evaporation
Metal contact	Al (200 nm) of 500 nm circular diameter on Si Au(200nm)/Ti(20nm) of 500 nm circular diameter on ZnO NRs

5.2.2 Structural, Surface Morphology and Optical Characterization of ZnO NRs

Well aligned uniformly distributed ZnO nanorods throughout silicon substrate were studied using FESEM and TEM images. Figure 5.12 (a-b) depicts FESEM images of top view and cross-section view of ZnO NRs, respectively. From the figure, it can be seen that NRs are self-aligned with circular diameter spread over the entire substrate. The calculated value of height, diameter, density and aspect ratio of ZnO NRs are ~ 750 nm, 48 nm, 1.26×10^{10} cm^{-2} and 15.62, respectively. For further confirmation of ZnO NRs existence, the ZnO NRs were removed from substrate by sonication in acetone and placed on TEM grids. TEM image and selected area electron diffraction (SAED) pattern are shown in Figure 5.12 (c-d). The diameter and heights of NRs in TEM images are very close to FESEM results. In SAED pattern, the presence of only bright spots confirms single crystalline nature of ZnO as we have seen in XRD spectra of these ZnO NRs [Xu *et al.*, 2012].

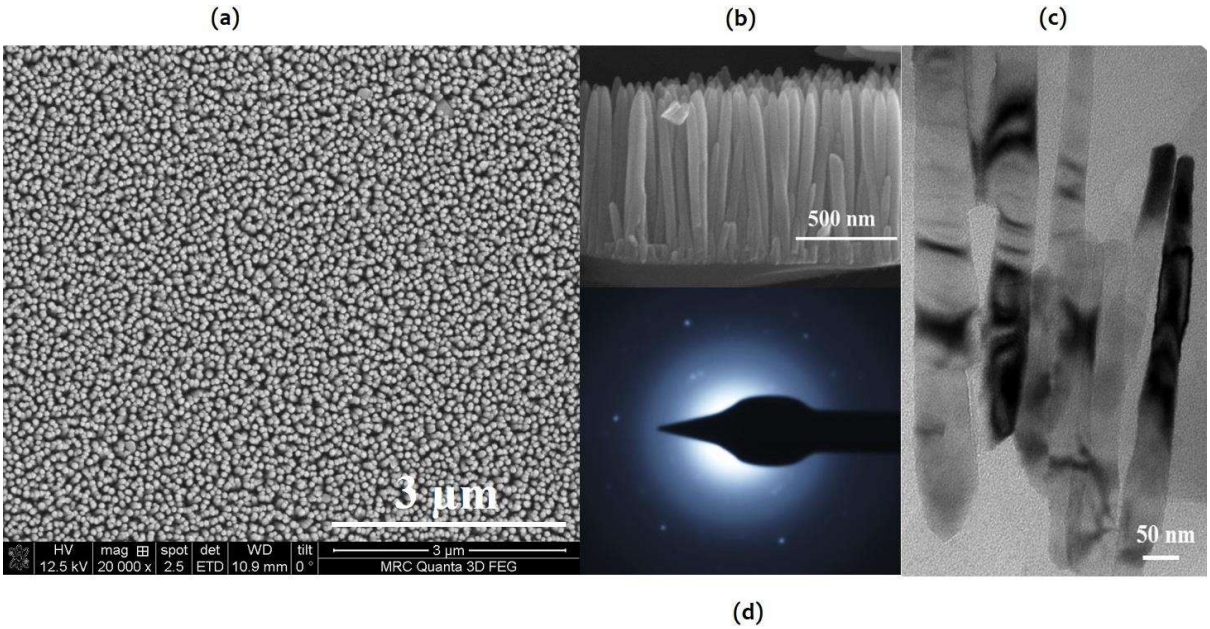

Figure 5.12: (a) Top view (b) Cross-sectional view of FESEM images of ZnO NRs, (c) TEM image and (d) SAED pattern of ZnO NR

In addition to the growth of almost defect free and highly crystalline ZnO, structural and optical characterization were also carried out. The 2θ-ω scan of XRD patterns shown in Figure 5.13 (a) depicts a strong peak at peak position of 2θ=34.64° with FWHM ~12 arcmin corresponding to (0002) diffraction of wurtzite ZnO. X-ray results clearly indicates that the NRs are grown along vertical [0002] direction to substrate as discussed in chapter 4. These deposited ZnO NRs were highly single crystalline as confirmed in SAED pattern of ZnO NRs.

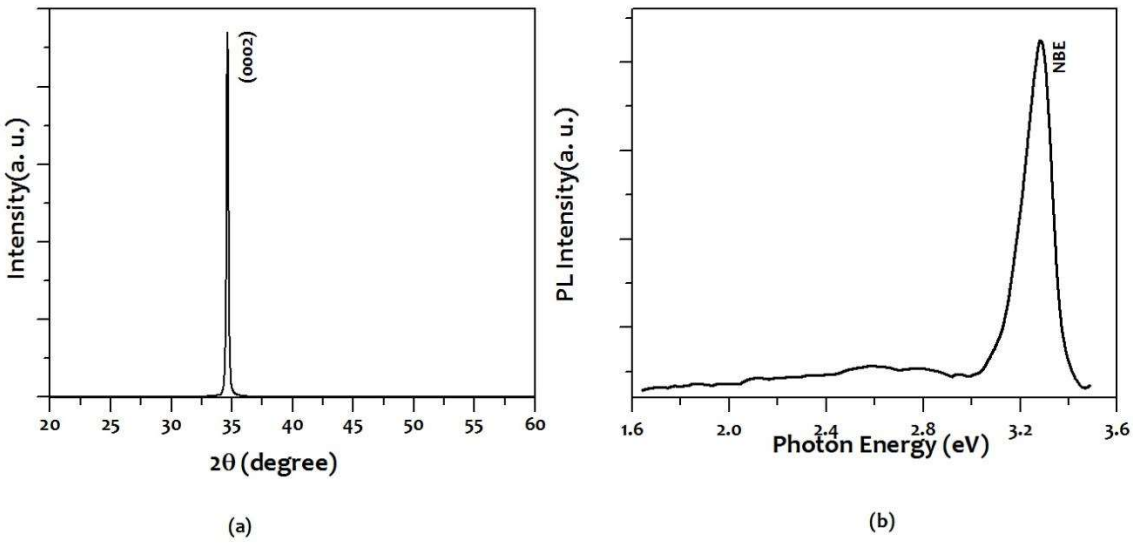

Figure 5.13: (a) X-Ray diffraction 2θ- ω scan, (b) Room temperature PL spectra

Room temperature PL spectra is shown in Figure 5.13 (b) and it shows a sharp peak around ~3.26 eV with FWHM 130 meV indexed near band emissions (NBE) transitions. Normally, a broad band emission peak in PL spectra at room temperature is observed due to the presence of structural defects [Chandrinou *et al.,* 2006]. Absence of broad band emission region in the PL spectra clearly indicates that the ZnO NRs are grown with minimal number of defect.

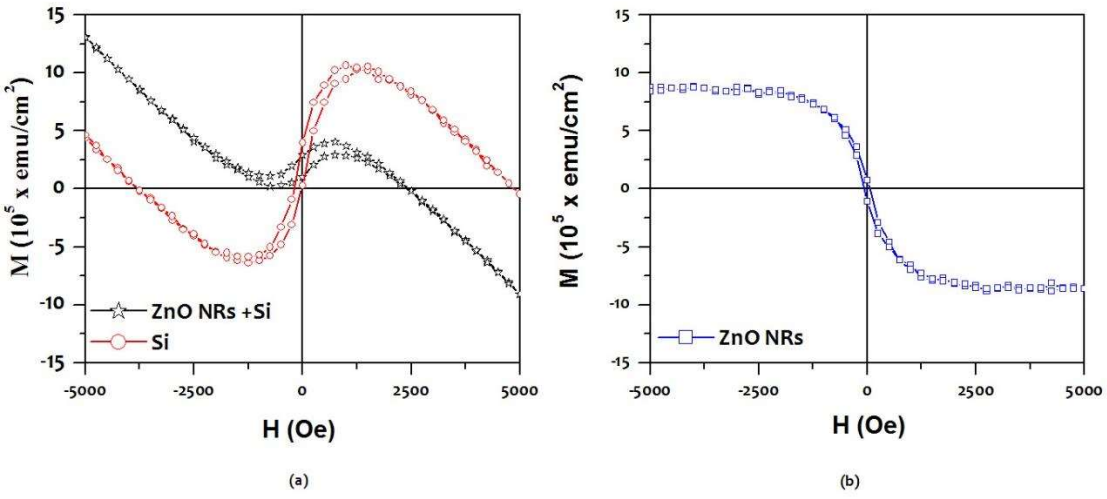

Figure 5.14: Magnetization versus magnetic field (M-H) curve for (a) ZnO NRs /Si and bare Si, and (b) ZnO NRs

Additionally, defect free growth of ZnO NRs were also verified by magnetic characterization using VSM study. Figure 5.14 (a) shows magnetization versus magnetic field (M-H) curve for ZnO NRs/n-Si and bare n-Si. After subtracting substrate contribution, ZnO NRs show diamagnetic behavior which has been shown in Figure 5.14 (b). Ferromagnetism is

observed in ZnO nanostructures due to the presence of oxygen vacancy defects [Sundaresan *et al.*, 2006]. The high temperature annealing performed on ZnO NRs in presence of oxygen showed ferromagnetic to diamagnetic behavior due to removal of oxygen vacancy defects [Panigrahy *et al.*, 2010].

5.2.3 Current Density with Voltage (J-V) Characteristics of ZnO NRs/Si Junction

The schematic diagram of ZnO NRs/n-Si single heterojunction (SHJ) and ZnO NRs/n-Si/ZnO NRs double heterojunctions (DHJs) are shown in Figure 5.15 (a). In this section, double heterojunction (DHJs) has been fabricated at interface of ZnO NRs/Si/ZnO NRs devices where Au/Ti ohmic contact was used for further removing any losses at contact. Figure 5.15 (b) shows schematic of energy band diagram for ZnO NRs/n-Si/ZnO NRs DHJs which illustrates electron transport mechanism at double Schottky barrier heights. While electrons gain sufficient energy to overcome Schottky barrier height, electrons flow from ZnO NRs to Si and then Si to ZnO NRs to complete current path. These DHJs devices shows same response in forward bias as well as in reverse bias condition as Si substrate is sandwiched between ZnO NRs.

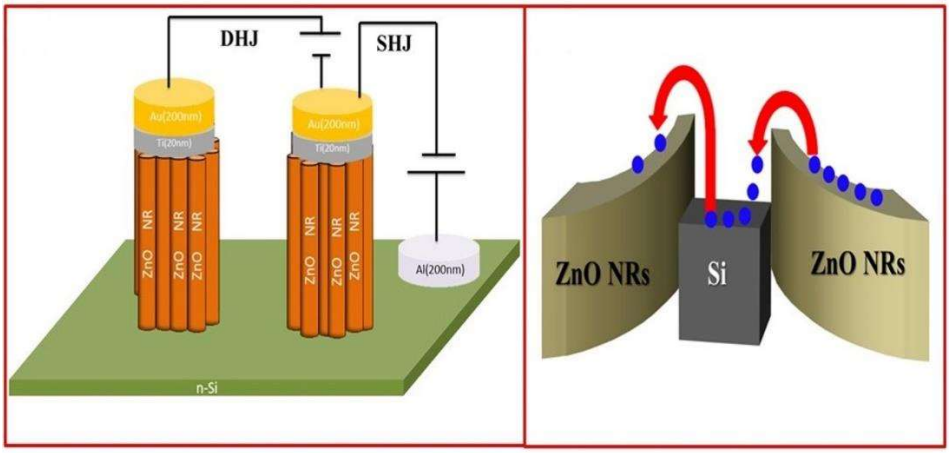

Figure 5.15: (a) The schematic diagram of ZnO NRs/n-Si single heterojunction (SHJ) and ZnO NRs/n-Si/ZnO NRs double heterojunctions (DHJs), (b) Schematic of energy band diagram for ZnO NRs/n-Si/ZnO NRs DHJs

Electrical transport studies at SHJ as well as DHJ were carried out using current density versus voltage characteristics at room temperature. Figure 5.16 (a) shows current density versus voltage (*J-V*) characteristics of SHJ and DHJs at room temperature. The observance of rectifying behavior in *J-V* curve of SHJ indicates the presence of Schottky barrier at junction as mentioned in former section of this chapter. The calculated value of rectification ratio was ~5.7 at 3 V with leakage current density 2.53 A/cm^2. In DHJs, current density also shows symmetric characteristic of *J-V* in forward and reverse bias due to symmetry in the device structure. Due to presence of Schottky barrier at junction, Schottky barrier's basic characteristics calculation such as ideality factor and barrier height is required. The Ideality factor (η) and barrier height (ϕ_B) of the SHJ and DHJs were calculated by using thermionic emission model by fitting linear region of current density in forward bias. Current density of these two heterojunctions is given below by equation [Roul *et al.*, 2011]:

$$J = J_o \left\{ \exp\left(\frac{qV}{\eta kT} \right) - 1 \right\} \tag{5.10}$$

where J_o is reverse saturation current density given by equation

$$J_o = A^* T^2 \exp\left(\frac{-q\phi_B}{kT} \right) \tag{5.11}$$

Here T, ϕ_B, k, A^*, and η are operating temperature, barrier height, Boltzmann constant, Richardson constant (112 $Acm^{-2}K^{-2}$ for n-Si) and Ideality factor, respectively. Figure 5.16 (b-c) shows linear region fitting in forward bias for ZnO NRs/n-Si SHJ and ZnO NRs/n-Si/ZnO NRs DHJs, respectively. Barrier height and ideality factor are calculated by thermionic emission model using equation 5.10 and 5.11. The fitted value of schottky barrier height and ideality factor was found to be ϕ_B=0.59 eV and η=3.4 for SHJ and ϕ_B=0.60 eV and η=3.5 for DHJs. Schottky barrier height of reverse bias of SHJ is also calculated using Bardeen model [Zhang and Harrell, 2003] and fitted plot for initial reverse bias value is shown in Figure 5.16 (d). Rakhshani *et al.* in [Rakhshani *et al.*, 1998] explained the Bardeen model as linear decay of barrier height when electric field increases. This model gives relation between reverse saturation current density at SHJ with respect to square root of applied reverse biased voltage as shown:

$$J = J_r \exp\left(\frac{\beta\sqrt{V_r}}{kT} \right) \tag{5.12}$$

where β is interface related parameter and J_r is given as reverse saturation current density which calculated as:

$$J_r = A^* T^2 \exp\left(\frac{-q\phi_r}{kT} \right) \tag{5.13}$$

Exponential fitting was used to calculate reverse barrier height (ϕ_r) as given in equation 5.14 which is comparable to equation 5.12

$$J = a \exp\left(b\sqrt{V} \right) \tag{5.14}$$

Where a is defined as reverse saturation current density. Reverse barrier height of SHJ was found to be ϕ_r =0.62 eV. Schottky barrier height is highly influenced by adsorbed/desorption of oxygen which enhances the sensitivity of the device. The DHJs plays an important role to enhance H_2 sensitivity or sensor response.

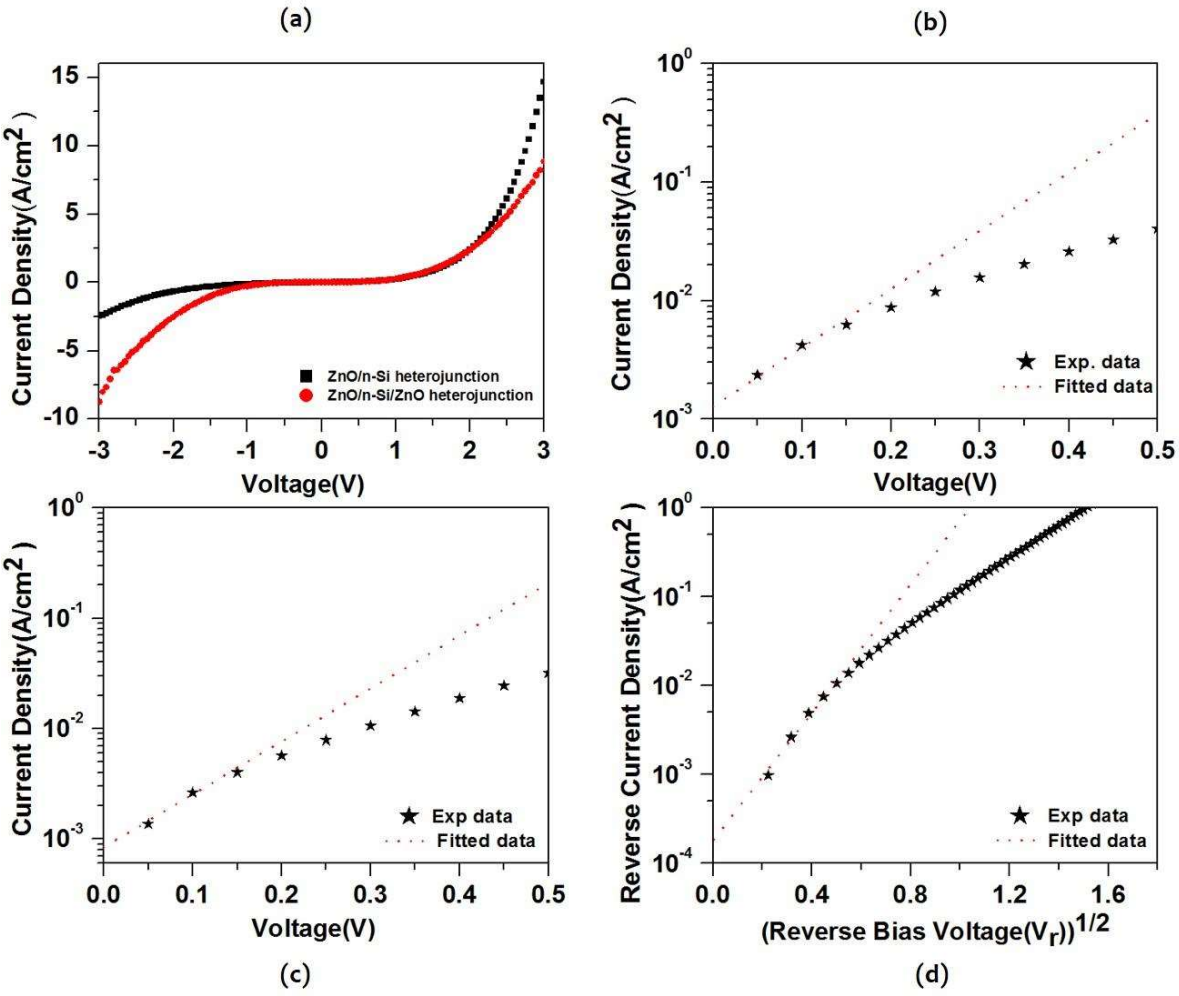

Figure 5.16: (a) Room temperature *J-V* characterization for ZnO NRs/Si SHJ and ZnO NRs/Si/ZnO NRs DHJs, (b)-(c) Linear fitting of forward bias region for SHJs and DHJs, respectively and (d) Extraction of Schottky barrier height of reverse bias of SHJs

5.2.4 Ohmic Contacted ZnO NRs/Si/ZnO NRs DHJ based Hydrogen Sensor

Hydrogen gas sensing properties of ZnO NRs were measured at pressure of about 2 x 10^{-3} mbar. Hydrogen sensing for ZnO depends on adsorption and desorption of environmental oxygen to form depletion region on NRs. When ZnO nanorods reacts with environmental oxygen and gases, its sensitivity (sensor response) towards gases changes and depends upon adsorbed oxygen (O^-, O^{2-}, O_2^-) ions and defects. Initially, when ZnO NRs are exposed to air, oxygen is adsorbed on surface of nanorods which leads to the extraction of electron from the conducting region of NRs and forms depletion region. Due to depletion region formation in NRs, its conduction channel area decreases which results in decrease in the conduction of the device. Electrical conduction (G) of ZnO NRs is strongly dependent on number of conducting electrons and is given by [Lupan *et al*., 2010]:

$$G = \frac{1}{R} = \frac{n|e|\mu\pi r^2}{l} \tag{5.15}$$

where *n, e, r, μ, l* are charge carrier concentration, electron charge, radius of NR, electron mobility and length of NR, respectively. Since, gas sensitivity is directly proportional to conduction cross-section channel area of NRs, channel area changes as depletion channel width

changes. At the time of hydrogen loading, negative oxygen ion reacts with H_2 and forms H_2O and releases electron into the layer. Thus, desorption of oxygen transfer electrons into NRs which leads to increase in the channel cross-section area and decrease in resistance. Sensitivity (sensors relative response) of gas sensor is defined as ratio of change in resistance in air with respect to H_2 gas as mentioned in chapter 1 [Gu *et al.*, 2012]. In this study, ZnO NRs/n-Si/ZnO NRs double Schottky junction were used for hydrogen detection at relatively low operating temperature. Resistive response of ZnO NRs /n-Si/ ZnO NRs were measured at 70°C in H_2 environment and shown in Figure 5.17 (a). In resistive response curve, during deloading of hydrogen in presence of environmental oxygen, sensor resistance increases towards base line. While in loading cycle, hydrogen molecule reacts with adsorbed oxygen ions and decreases depletion channel width in ZnO NRs which tends to decrease sensor resistance towards saturation. The variation in the minimum value of resistance in case of first and second cycle is ~ 2.5%, whereas, for other cycles is ~ ±0.5%. The charges (O^{2-} ions) on the surface of ZnO NRs are not completely released in the first cycle, while in second cycle, it removes most of the O^{2-} ions and changes the minimum value of resistance. Also, there is possibility that some hydrogen atoms are trapped in the NRs in first cycle and dimension of the NR itself might be changed due to swelling in the NR [Favier *et al.*, 2001]. As a consequence, the dimension of NRs also increases which decreases the resistance in second cycle.

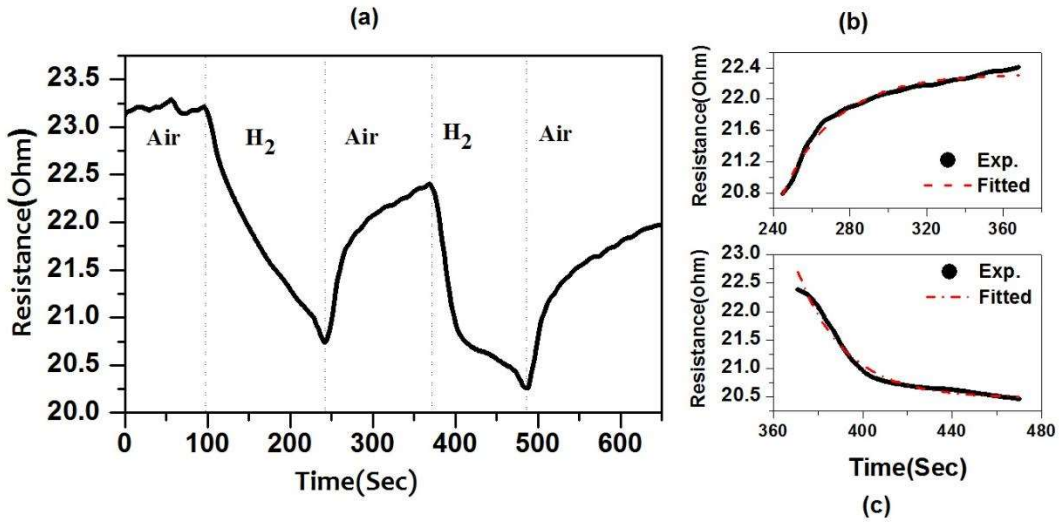

Figure 5.17: (a) Resistivity response of ZnO NRs/Si/ZnO NRs device at 70°C for pure hydrogen and (b), (c) Exponential fitting of resistivity response curve for recovery and response time, respectively

Response time, recovery time and sensitivity (relative response) are three key parameters for any gas sensor. The response time or decay time (τ_d) represents change in 90% of saturation resistance with loading of hydrogen, while deloading of hydrogen gas through chamber shows exponentially increase in resistance response and gives recovery or rise time (τ_r). Figure 5.17 (b-c) gives exponential fitting of response curve for the decay and rise time which is given as [Adamyan *et al.*, 2009]:

$$R = R_0 + A\exp\left(\frac{t}{\tau_r}\right) \tag{5.16}$$

$$R = R_1 + B\exp\left(-\frac{t}{\tau_d}\right) \quad (5.17)$$

Where A and B are scaling constant. From these fitting, rise and decay time constant were calculated as 27 sec and 21 sec respectively, which shows fast response and recovery time at relatively low operating temperature. Tien *et al.* in [Tien et al., 2005], conveyed three times higher response time for ZnO NRs in comparison to ZnO thin film. Sensitivity (relative change in resistance) of ZnO NRs /n-Si/ ZnO NRs sensor was found to be ~10.05% in the presence of pure hydrogen. There are many reports on ZnO nanostructure based hydrogen sensor with high sensitivity where operating temperature was kept above 150 °C. Al-Salman *et al.* in [Al-Salman and Abdullah, 2013], described ZnO nanostructure based H_2 sensor, having high defect density and operated at 200 °C which shows high sensitivity. In this study, ZnO NRs are defect free and showed high sensitivity for H_2 gas at low operating temperature.

5.2.5 Proposed Hydrogen Gas Sensing Mechanism

Based on experimental observation, a gas sensing mechanism is proposed and shown in Figure 5.18 where chemisorbed oxygen ions totally depends on operating temperature. At lower temperature, O^{2-} ions are dominantly adsorbed by NRs but at higher temperature (>150°C) these ion are negligible and O^{-} ions are dominantly adsorbed. When NRs interact with oxygen, they form a depletion region and decreases resultant channel diameter of conduction. During the loading of H_2, H_2 reacts with oxygen ion and increases channel diameter and as a result the channel resistance decreases [Hsu *et al.*, 2014]. Figure 5.18 (a-c) shows schematic diagram of gas sensing mechanism of lesser number of defects in ZnO NRs, defect contained ZnO NRs at low and high (>150 °C) operating temperatures, respectively. Due to presence of defects at low temperature, hydrogen reaction on NRs increases channel diameter but is still minor as compared to high temperature operation as shown in Figure 5.18. Since, higher energy or temperature is required to completely remove the adsorbed oxygen from defect points, it can be said that gas sensitivity could be higher in the presence of defects at high operating temperature (>150 °C) due to larger conduction region [Nan *et al.*, 2014]. However, at low operating temperature, sensitivity could be lower in presence of defects in NRs which increases depletion region. At low operating temperature, intrinsic defects were not completely removed from conduction region of ZnO NRs due to which NRs depletion region was increased in comparison to high operating temperature depletion region. In this study, almost defect-free ZnO NRs (lesser number of defects) were grown, which gave high relative response even at low temperature. In this approach, while hydrogen loading, adsorbed oxygen ions completely reacts with hydrogen molecules and releases conduction electron and reduces depletion channel width to large extent. As we have mentioned that there are almost negligible structural defects present in ZnO NRs, it achieves high sensor response in comparison to ZnO NRs with defects at low operating temperature. Consequently, low dimensional structures can be used at low temperature for hydrogen gas sensor. Thus, a mechanism is imparted to fabricate hydrogen sensors, which can operate at low temperature unlike the existing hydrogen sensors, which operate at high temperature.

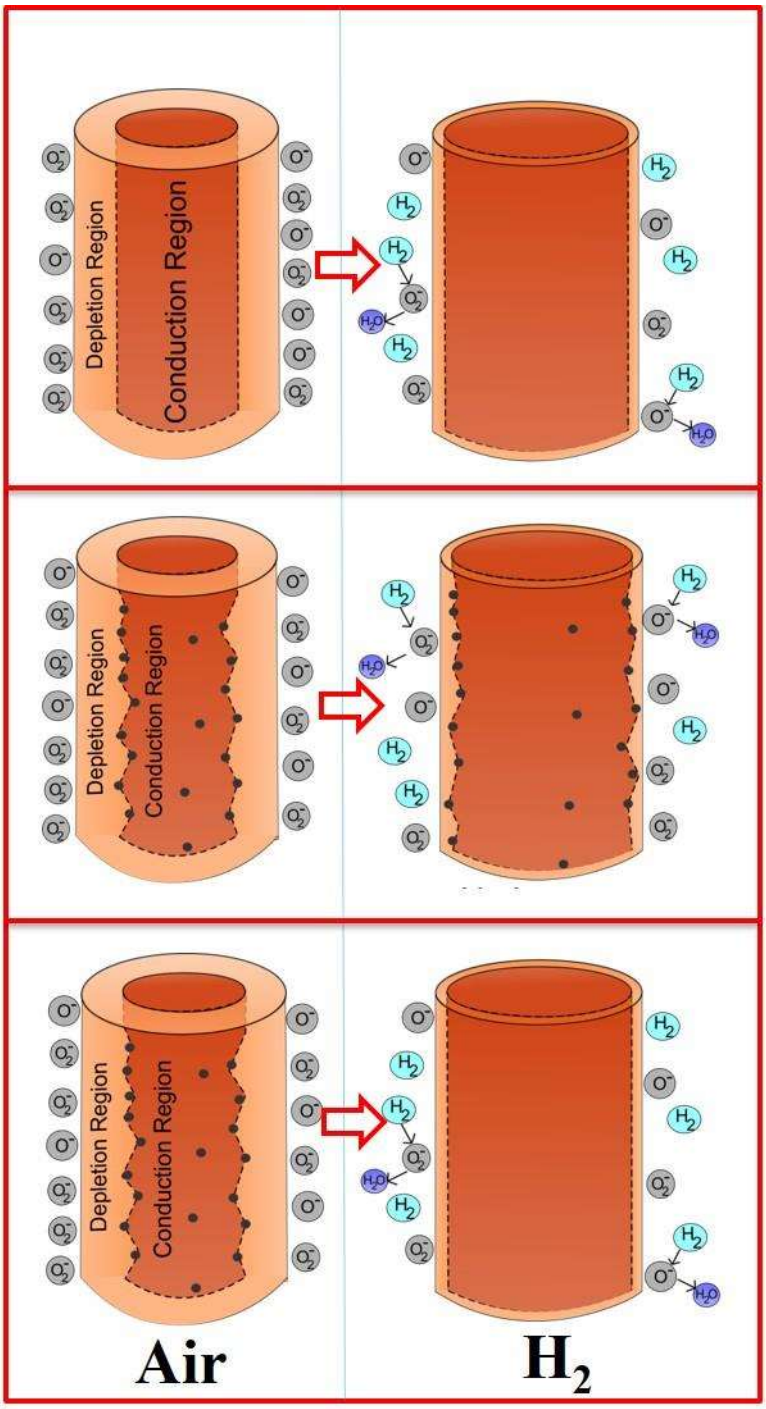

Figure 5.18: Schematic diagram of gas sensing mechanism of ZnO NRs: (a) lesser number of defects, (b) ZnO NRs with defects at low temperature (<150 °C) and (c) ZnO NRs with defects at High (>150 °C) operating temperatures, respectively

5.3 CONCLUSION

To conclude, Electrical *I-V* characterization of ZnO NRs/Si HJ were investigated in the range of 120-300 K. Ideality factor and barrier height of the HJ were estimated from TE and were found to be highly temperature dependent in nature due to the presence of defects and barrier inhomogeneities at junction. Double Gaussian distribution of barrier height with thermionic emission gives mean barrier heights 0.55 eV and 0.86 eV for two different temperature regions 120-180 K and 210-300 K, respectively. Modified Richardson constant ~123 $Acm^{-2}K^{-2}$ in the temperature range of 210-300K is close to theoretical value of n-Si. In addition to this, Ohmic

contacted ZnO NRs based hydrogen sensor were fabricated. Double Schottky junction enhances sensor response of the device. The device is found to have fast response of ~21.6 s and recovery time of ~27 s during loading/deloading of pure hydrogen because of high aspect ratio and uniformity of nanorods. This sensor setup gives sensors response S of ~10.05% at the operating temperature of 70 ^{o}C.

…